Image Boundary Extension with Mean Value for Cosine-Sine Modulated Lapped/Block Transforms

Ryoma Ishibashi, Taizo Suzuki, *Senior Member, IEEE*, Seisuke Kyochi, *Member, IEEE*, and Hiroyuki Kudo, *Member, IEEE*

***Abstract*—We present a novel image boundary extension, mean value extension (MVE), for directional lapped transforms, particularly cosine-sine modulated lapped transforms (CSMLTs). Lapped transforms are usually used with an extension technique, such as periodic extension (PE) or symmetric extension (SE), for nonexpansive convolution at signal boundaries. When directional textures (oblique lines and curves) appear at the 2D signal (image) boundaries, both PE and SE produce directional discontinuities, which degrade the sparsity of the transformed coefficients, especially in the case of directional lapped transforms. MVE reduces the discontinuities for directional textures better than PE or SE do; it thus improves the efficiency of the sparse representation based on directional lapped transforms. Moreover, to reduce computational costs compared with those of directional lapped transforms, we introduce new directional block transforms, called cosine-sine modulated block transforms (CSMBTs). These new transforms are derived from a minimum tile processing (tiling) of M-band CSMLTs with $2M$ filter lengths and nonexpansive convolutions. The resulting directional block transforms, particularly in the case of the MVE, have richer directional selectivity and have higher performance compared with a discrete Fourier transform (DFT) as shown in experiments.**

***Index Terms*—Cosine-sine modulation, directional block transforms, directional lapped transform, mean value extension, nonexpansive convolution.**

I. Introduction

DISCRETE cosine transforms (DCTs) [1] and discrete wavelet transforms (DWTs) [2] are widely used for various types of image processing, e.g., image restoration (denoising, deblurring, and so on) and in the image/video coding standard JPEG [3], the H.26x series [4], [5], and JPEG 2000 [6]). However, since atoms (i.e., elements of basis/frames) of DWTs are lying only horizontal and vertical directions (and components mixing ± 45 degree directions); they cannot directly express directional features such as oblique lines and curves. Thus, they are often referred to as having poor directional selectivity [7]; i.e., they cannot provide efficient sparse representations for directional textures.

Directional transforms, which can express rich directional textures sparsely, have been extensively studied. They are classified into two classes. The first class, so-called "adaptive directional transforms" [8]–[12], typically does not have directional atoms except for vertical and horizontal directions (as in DCT and DWT), but they are applied to images along predetermined oblique directions (the direction can be changed at every pixel). However, the applications of adaptive directional transforms are relatively limited because, for example in image recovery, it is difficult to determine suitable directions from a degraded input image contaminated by noise, blur, pixel missing, and so on. Another one is a class of transforms of which atoms are lying along various directions. Since the applications of the directional transforms with directional atoms cover general applications including signal recovery, we focus on them and will call them "directional transforms." They are further classified into directional lapped transforms (such as *curvelet* [13], *ridgelet* [14], and *contourlet* [15], and the multidimensional nonseparable lapped transforms [16]–[18]) and directional block transforms (such as discrete Fourier transform (DFT) [19]). Directional lapped transforms are directional transforms with the atoms of which supports are lapped each other, while directional block transforms are directional transforms with the atoms of which supports are not lapped.

Among them, *dual-tree complex wavelet transforms* (DT$\mathbb{C}$WTs) [7] have been paid much attention to because of their low computational complexity and rich directional selectivity. Their directional functions in the frame are generated by using two parallel maximally decimated filter banks (FBs) satisfying the half-sample delay condition [20]. One problem with DT$\mathbb{C}$WTs is that, since the half-sample delay condition is difficult to approximate with finite impulse response (FIR) filtering, the resulting filter performance characteristics, such as stopband attenuation and coding gain, are often degraded, especially with short filter lengths. To solve this problem, cosine-sine modulated lapped transforms (CSMLTs)[1] have been widely studied [21]–[24] as an alternative class of DT$\mathbb{C}$WTs.[2] CSMLTs can be easily designed by modulating a prototype lowpass filter instead of approximating the half-sample delay condition, and they work better than DT$\mathbb{C}$WTs do in image processing, e.g., image denoising [23], [24].

The CSMLTs are lapped transforms which have longer

R. Ishibashi is with NEC Corporation, Minato-ku, Tokyo, 108-8001 Japan (e-mail: r-ishibashi@bu.jp.nec.com).

T. Suzuki and H. kudo are with the Faculty of Engineering, Information and Systems, University of Tsukuba, Tsukuba, Ibaraki, 305-8573 Japan (e-mail: {taizo, kudo}@cs.tsukuba.ac.jp).

S. Kyochi is with the Department of Information and Media Engineering, The University of Kitakyushu, Kitakyushu, Fukuoka, 808-0135 Japan (e-mail: s-kyochi@kitakyu-u.ac.jp).

[1]Although they are often called cosine-sine modulated FBs (CSMFBs), we will call them CSMLTs to clearly distinguish them from block transforms.

[2]Modulated complex lapped transform (MCLT) in [25] is essentially the same transform as the CSMLTs because they are also designed by the modulation of a prototype filter (the definition in the cosine and sine modulation terms is slightly different). However, the MCLT has been introduced as a 1D complex-valued transform for effective audio processing in [25]. On the other hand, the CSMLTs has been firstly introduced as a directional selective 2D real-valued transform for effective image processing in [21].

filter lengths L than the number of bands (or band count) M ($M, L \in \mathbb{N}$, $L > M$) and require extra signals for perfect reconstruction (PR) at boundaries. Nonexpansive convolution, e.g., periodic extension (PE) and symmetric extension (SE) [26], is one of the simplest approaches to solving the boundary problem. PE often causes discontinuities at boundaries, whereas SE typically extends the boundaries more smoothly. There are also other smooth nonexpansive convolutions for various FBs [27]–[29]. However, when the conventional nonexpansive convolution methods are applied to images involving directional textures at boundaries, "directional" lapped transforms such as CSMLTs cannot provide efficient sparse representations at image boundaries. Thus, in image restoration for example, this often results in annoying artifacts near the boundaries.

Here, we present a nonexpansive convolution, called mean value extension (MVE), that can simply reduce discontinuities at boundaries by extending with the mean value of the pixels located near the boundaries. Unlike PE and SE, this extension requires a lattice structure implementation of FBs for its execution. Since, as will be illustrated in this paper, the CSMLTs can be designed with a lattice structure implementation [30], MVE can be incorporated with them.

We further introduce new directional block transforms, called cosine-sine modulated block transforms (CSMBTs), derived from a minimum tile processing (tiling) of CSMLTs with $2M$ filter lengths and nonexpansive convolutions. Block transforms with a filter length L equal to the number of bands M ($L = M$) generally have lower computational costs than lapped transforms do, and their computations for every block in an input image can be fully parallelized. The DCT and discrete sine transform (DST) [1] are efficient block transforms, and they are used in many applications, such as JPEG and the H.26x series. However, they cannot analyze various directions because, like DWTs, their basis suffers from poor directional selectivity. On the other hand, the DFT is the most-used "directional" block transform. One problem with the DFT is that some atoms in its basis have the same directions. Thus, the number of directions is limited. Since the new CSMBTs, especially in the case of MVE, have richer directional selectivity, they are expected to work better than the DFT in various image processing applications.

A preliminary version of this paper was presented in [31], where we discussed only the MVE for M-band CSMLTs with a filter length of $2M$. This paper describes the general case of a filter length L longer than the number of bands M. Moreover, it discusses how the MVE is used in the design of CSMBTs.

The remainder of the paper is organized as follows. Section II reviews the traditional directional block transforms and CSMLTs. Section III presents MVE and derives the CSMBTs. Section IV compares the resulting transforms with the conventional methods. Section V concludes this paper.

Notation: Boldface lower- and upper-case letters represent vectors and matrices, respectively. The number of bands M is technically constrained to an even number. The set of $M \times N$ real-valued matrices is denoted as $\mathbb{R}^{M\times N}$. For $\mathbf{A} \in \mathbb{R}^{M\times M}$, $[\mathbf{A}]_\times \in \mathbb{R}^{\frac{M}{2}\times\frac{M}{2}}$ ($\times = \alpha, \beta, \gamma, \text{or} \delta$) is the submatrix,

$$\mathbf{A} = \begin{bmatrix} [\mathbf{A}]_\alpha & [\mathbf{A}]_\beta \\ [\mathbf{A}]_\gamma & [\mathbf{A}]_\delta \end{bmatrix}. \tag{1}$$

$\mathbf{A}^\top$ is the transpose of the matrix $\mathbf{A}$. $\mathrm{diag}(a_0, \cdots, a_{M-1})$ and $\mathrm{diag}(\mathbf{A}_0, \cdots, \mathbf{A}_{M-1})$ are $M \times M$ diagonal and block diagonal matrices whose diagonal elements are $a_0, \cdots, a_{M-1}$ and $\mathbf{A}_0, \cdots, \mathbf{A}_{M-1}$, respectively. $\mathbf{I}$, $\mathbf{J}$, and $\mathbf{O}$ indicate the identity matrix, the reversal identity matrix, and the zero matrix, respectively. A diagonal matrix $\mathbf{D}$ is defined as $\mathbf{D} = \mathrm{diag}(1, -1, \cdots, 1, -1)$. j is the unit complex number $\sqrt{-1}$. $\bar{c}$ is the conjugate of $c \in \mathbb{C}$. $H(z)$ and $\widetilde{H}(z)$ are defined as $H(z) = \sum_n h(n) z^{-n}$ and $\widetilde{H}(z) = \sum_n \overline{h(n)} z^n$, respectively. $H(\omega) = H(e^{j\omega})$. An $M \times L$ transform is a transform with number of bands M and filter length L.

II. Review and Definitions

A. Directional Block Transforms

The DFT [19] is expressed for an M-sample finite discrete signal $x(n)$ as

$$X(m) = \frac{1}{\sqrt{M}} \sum_{n=0}^{M-1} x(n) e^{-j\frac{2\pi mn}{M}} \quad \text{for} \quad 0 \le m \le M-1. \tag{2}$$

This transform can be equivalently expressed as $\widehat{\mathbf{x}} = \boldsymbol{\mathcal{F}}\mathbf{x}$, where $\mathbf{x}$ and $\widehat{\mathbf{x}}$ are $M \times 1$ input and output signals, respectively, and the (m, n)th-element of the M-band DFT matrix $\boldsymbol{\mathcal{F}}$ is defined as

$$[\boldsymbol{\mathcal{F}}]_{m,n} = \frac{1}{\sqrt{M}} e^{-j\frac{2\pi mn}{M}}. \tag{3}$$

The DCT and DST [1] come in various types. The (m, n)th-elements of the M-band type-II DCT (DCT-II) matrix $\boldsymbol{\mathcal{C}}_{II}$, which is used in JPEG and the H.26x series, type-II DST (DST-II) matrix $\boldsymbol{\mathcal{S}}_{II}$, type-IV DCT (DCT-IV) matrix $\boldsymbol{\mathcal{C}}_{IV}$, and type-IV DST (DST-IV) matrix $\boldsymbol{\mathcal{S}}_{IV}$ are respectively defined as

$$[\boldsymbol{\mathcal{C}}_{II}]_{m,n} = \sqrt{\frac{2}{M}} s_m \cos\frac{\pi m(n+1/2)}{M} \tag{4}$$

$$[\boldsymbol{\mathcal{S}}_{II}]_{m,n} = \sqrt{\frac{2}{M}} s'_m \sin\frac{\pi (m+1)(n+1/2)}{M} \tag{5}$$

$$[\boldsymbol{\mathcal{C}}_{IV}]_{m,n} = \sqrt{\frac{2}{M}} \cos\frac{\pi (m+1/2)(n+1/2)}{M} \tag{6}$$

$$[\boldsymbol{\mathcal{S}}_{IV}]_{m,n} = \sqrt{\frac{2}{M}} \sin\frac{\pi (m+1/2)(n+1/2)}{M}, \tag{7}$$

where

$$s_m = \begin{cases} \frac{1}{\sqrt{2}} & (m = 0) \\ 1 & (m \ne 0) \end{cases}$$

$$s'_m = \begin{cases} \frac{1}{\sqrt{2}} & (m = M-1) \\ 1 & (m \ne M-1) \end{cases}.$$

The separable 2D DCT and DST do not exhibit directional orientation. For example, each 2D DCT-II atom $C_{n_1,n_2}^{(m_1,m_2)}$ forms

$$C_{n_1,n_2}^{(m_1,m_2)} = s_{m_1} s_{m_2} \frac{2}{M} \cos\vartheta_{m_1,n_1} \cos\vartheta_{m_2,n_2}, \tag{8}$$

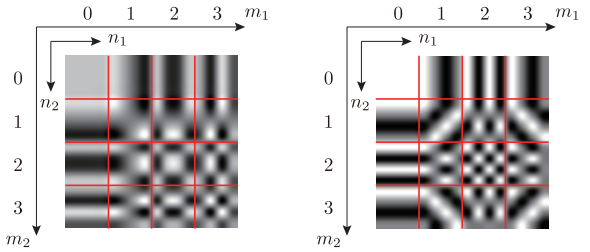

Fig. 1: Atoms in basis ($M = 4$): (a) DCT-II, (b) DFT (real part).

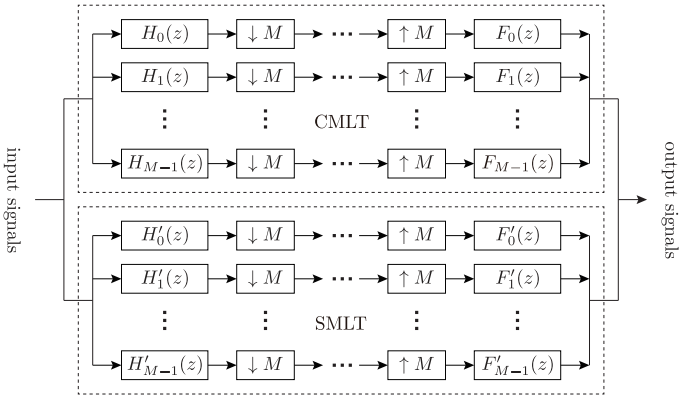

Fig. 2: M-band CSMLTs.

where m_1 and n_1 denote vertical subband/spatial indices, m_2 and n_2 denote horizontal ones ($m_1, m_2, n_1, n_2 \in \{0, \cdots, M-1\}$), and

$$\vartheta_{m,n} = \frac{\pi m(n+1/2)}{M}.$$

Fig. 1(a) shows examples of DCT atoms.[3] Clearly, they are not directionally oriented and cannot express various directional components. On the other hand, each 2D DFT atom $F_{n_1,n_2}^{(m_1,m_2)}$ forms

$$F_{n_1,n_2}^{(m_1,m_2)} = \frac{1}{M} e^{j\left(\varphi_{m_1,n_1}+\varphi_{m_2,n_2}\right)}, \tag{9}$$

where

$$\varphi_{m,n} = \frac{2\pi mn}{M}.$$

As shown in Fig. 1(b), the basis contains directionally oriented atoms. One problem with the 2D DFT is that its basis contains duplicate atoms and it cannot provide rich directional selectivity, as shown in Fig. 1(b). This follows from the fact that

$$\overline{e^{j\left(\varphi_{m_1,n_1}+\varphi_{m_2,n_2}\right)}} = e^{j\left(\varphi_{M-m_1,n_1}+\varphi_{M-m_2,n_2}\right)}. \tag{10}$$

Hence, when used in image analysis and processing, DFTs often degrade the efficiency of image analysis and processing.

B. Cosine-Sine Modulated Lapped Transforms (CSMLTs)

CSMLTs are an alternative class of DT$\mathbb{C}$WTs with rich directional selectivity. Unlike DT$\mathbb{C}$WTs, they do not require the half-sample delay condition. Instead, they are constructed from two M-band parallel FBs, which are designed by performing cosine and sine modulations on a prototype filter $p(n)$, i.e., by applying cosine and sine modulated lapped transforms (CMLT and SMLT).

[3] In Fig. 1, each atom is enlarged for visualization.

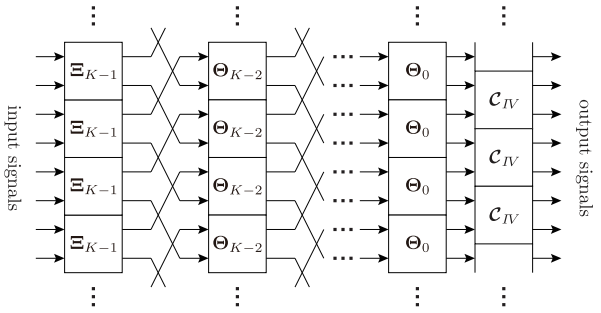

Fig. 3: Time-series processing of lattice structure of M-band CMLT (arrows indicate $M/2$ signals).

1) CMLT and SMLT: The CMLT and SMLT are shown in Fig. 2 [32]. The filter coefficients of $H_m(z)$, $F_m(z)$, $H'_m(z)$, and $F'_m(z)$ ($0 \le m \le M-1$) are expressed as follows [21]:

$$h_m(n) = 2p(n)\cos\left(\phi_{m,n} + \psi_m\right) \tag{11}$$
$$f_m(n) = 2p(n)\cos\left(\phi_{m,n} - \psi_m\right) \tag{12}$$
$$h'_m(n) = 2p(n)\sin\left(\phi_{m,n} + \psi_m\right) \tag{13}$$
$$f'_m(n) = 2p(n)\sin\left(\phi_{m,n} - \psi_m\right), \tag{14}$$

where

$$\phi_{m,n} = \left(m + \frac{1}{2}\right)\frac{\pi}{M}\left(n - \frac{L-1}{2}\right)$$
$$\psi_m = (-1)^m \frac{\pi}{4}$$

and L is the length of the prototype filter $p(n)$. The condition on the prototype filter $p(n)$ for PR is [32]

$$\widetilde{G}_\ell(z)G_\ell(z) + \widetilde{G}_{M+\ell}(z)G_{M+\ell}(z) = \frac{1}{2M} \quad \left(0 \le \ell \le \frac{M}{2} - 1\right), \tag{15}$$

where $G_\ell(z)$ ($0 \le \ell \le 2M-1$) are the polyphase components of the prototype filter $P(z)$, i.e.,

$$P(z) = \sum_{\ell=0}^{2M-1} G_\ell(z^{2M}) z^{-\ell},$$

where

$$G_\ell(z) = \sum_n p(2Mn + \ell) z^{-n}.$$

The CMLT and SMLT with the prototype filter $p(n)$ can be represented as the following lattice structure of the polyphase matrices by using the symmetry of cosine/sine modulation terms $\cos(\phi_{m,n} \pm \psi_m)$ and $\sin(\phi_{m,n} \pm \psi_m)$ in (11)-(14) and the PR condition in (15). Let $\mathbf{E}_{\mathcal{C}}(z)$ and $\mathbf{E}_{\mathcal{S}}(z)$ be the polyphase matrices of an $M \times 2KM$ ($K \in \mathbb{N}$) CMLT and SMLT, respectively. The relationship between two polyphase matrices

is $\mathbf{E}_{\mathcal{S}}(z) = z^{-\ell}\mathbf{D}\widetilde{\mathbf{E}_{\mathcal{C}}}(z)$, $\ell \in \mathbb{Z}$. If the CMLT satisfies the PR condition, the SMLT also satisfies it. The polyphase matrix $\mathbf{E}_{\mathcal{C}}(z)$ based on DCT-IV $\boldsymbol{\mathcal{C}}_{IV}$ can be expressed as a lattice structure (see Fig. 3) [30]:

$$\mathbf{E}_{\mathcal{C}}(z) = \boldsymbol{\mathcal{C}}_{IV}\mathbf{W}\boldsymbol{\Lambda}(z)\boldsymbol{\Theta}_0\left(\prod_{k=1}^{K-1}\boldsymbol{\Lambda}\left(z^2\right)\boldsymbol{\Theta}_k\right)\mathbf{J}, \tag{16}$$

where

$$\boldsymbol{\Theta}_i = \begin{bmatrix} -\mathbf{C}_i & \mathbf{S}_i\mathbf{J} \\ \mathbf{J}\mathbf{S}_i & \mathbf{J}\mathbf{C}_i\mathbf{J} \end{bmatrix},\ \mathbf{W} = \begin{bmatrix} \mathbf{O} & \mathbf{I} \\ \mathbf{I} & \mathbf{O} \end{bmatrix},\ \boldsymbol{\Lambda}(z) = \begin{bmatrix} z^{-1}\mathbf{I} & \mathbf{O} \\ \mathbf{O} & \mathbf{I} \end{bmatrix}$$
$$\mathbf{C}_i = \operatorname{diag}\left(\cos\theta_{i,0}, \ldots, \cos\theta_{i,M/2-1}\right)$$
$$\mathbf{S}_i = \operatorname{diag}\left(\sin\theta_{i,0}, \ldots, \sin\theta_{i,M/2-1}\right)$$

and θ_i is a free parameter for $0 \le i \le K-1$. Let

$$\boldsymbol{\Xi}_{K-1} \triangleq \boldsymbol{\Theta}_{K-1}\mathbf{J} \tag{17}$$

for later discussion. Another polyphase matrix $\mathbf{E}_{\mathcal{S}}(z)$ based on DST-IV $\boldsymbol{\mathcal{S}}_{IV}$ is

$$\mathbf{E}_{\mathcal{S}}(z) = \boldsymbol{\mathcal{S}}_{IV}\mathbf{W}\boldsymbol{\Lambda}(z)\boldsymbol{\Theta}'_0\left(\prod_{k=1}^{K-1}\boldsymbol{\Lambda}\left(z^2\right)\boldsymbol{\Theta}'_k\right)\mathbf{J}, \tag{18}$$

where

$$\boldsymbol{\Theta}'_i = \begin{bmatrix} \mathbf{C}_i & \mathbf{S}_i\mathbf{J} \\ \mathbf{J}\mathbf{S}_i & -\mathbf{J}\mathbf{C}_i\mathbf{J} \end{bmatrix} = \begin{bmatrix} \mathbf{I} & \mathbf{O} \\ \mathbf{O} & -\mathbf{I} \end{bmatrix}\boldsymbol{\Theta}_i\begin{bmatrix} -\mathbf{I} & \mathbf{O} \\ \mathbf{O} & \mathbf{I} \end{bmatrix}.$$

2) CSMLTs as 2D Directional Lapped Transform: The directional selectivity arising from CSMLTs can be explained as follows. Let $U_m(\omega)$ and $V_m(\omega)$ be a complex combination of spectra between $H_m(\omega)$ and $H'_m(\omega)$,

$$\begin{aligned} U_m(\omega) &= H_m(\omega) + jH'_m(\omega) \\ &= e^{j\eta_k}\sum_{n=0}^{L-1} p(n)e^{-j\left(\omega-\left(m+\frac{1}{2}\right)\frac{\pi}{M}\right)n} \\ &= e^{j\eta_k}P\left(\omega - \left(m+\frac{1}{2}\right)\frac{\pi}{M}\right), \end{aligned} \tag{19}$$

$$\begin{aligned} V_m(\omega) &= \frac{1}{j}\left(H_m(\omega) - jH'_m(\omega)\right) \\ &= e^{-j\eta_k}P\left(\omega + \left(m+\frac{1}{2}\right)\frac{\pi}{M}\right), \end{aligned} \tag{20}$$

where

$$\eta_k = -\left(m+\frac{1}{2}\right)\frac{\pi}{M}\frac{L-1}{2} + (-1)^m\frac{\pi}{4}.$$

Since $U_m(\omega)$ and $V_m(\omega)$ are the modulations of a prototype lowpass filter $P(\omega)$, each frequency response is one-sided in the positive or negative frequency domain. The frequency responses of $U_m(\omega)$ and $V_m(\omega)$ in the case of

$$p(n) = -\sin\left(\frac{\pi}{2M}\left(n+\frac{1}{2}\right)\right) \tag{21}$$

for $0 \le n \le 2M-1$, which satisfies the PR condition in (15) and generates a lapped transform with maximum DC concentration [33], are shown in Fig. 4(a). From (19) and (20), we can derive the following 2D frequency spectra:

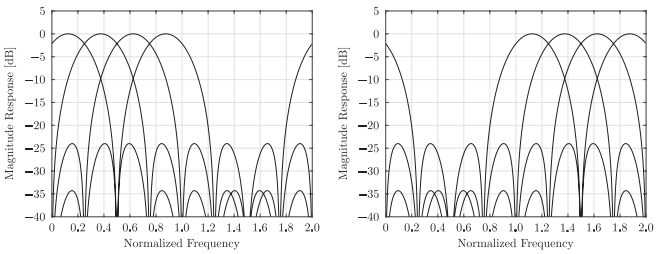

(a)

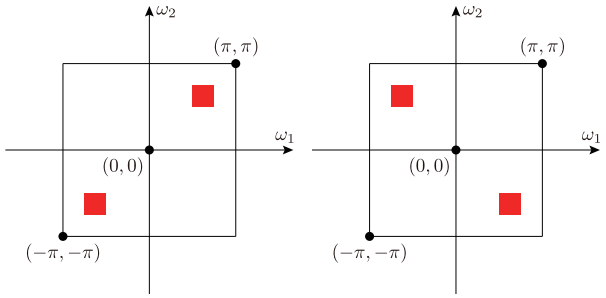

(b)

Fig. 4: Frequency responses of 4×8 CSMLTs ($[0, 2\pi]$): (a) $H_m(\omega) + jH'_m(\omega)$ and $H_m(\omega) - jH'_m(\omega)$, (b) $U_{m_1}(\omega_1)U_{m_2}(\omega_2) + V_{m_1}(\omega_1)V_{m_2}(\omega_2)$ and $U_{m_1}(\omega_1)V_{m_2}(\omega_2) + V_{m_1}(\omega_1)U_{m_2}(\omega_2)$, where $m, m_1, m_2 \in \{0, 1, 2, 3\}$.

$$\begin{aligned} &U_{m_1}(\omega_1)U_{m_2}(\omega_2) + V_{m_1}(\omega_1)V_{m_2}(\omega_2) \\ &= H_{m_1}(\omega_1)H_{m_2}(\omega_2) - H'_{m_1}(\omega_1)H'_{m_2}(\omega_2) \end{aligned} \tag{22}$$

$$\begin{aligned} &U_m(\omega_1)V_m(\omega_2) + V_m(\omega_1)U_m(\omega_2) \\ &= H_{m_1}(\omega_1)H_{m_2}(\omega_2) + H'_{m_1}(\omega_1)H'_{m_2}(\omega_2). \end{aligned} \tag{23}$$

This indicates that directional spectra of the (1,3)-quadrant and (2,4)-quadrant can be generated by performing additions and subtractions between the transform coefficients obtained by the separable 2D CMLT and SMLT, as shown in Fig. 4(b). The construction of the 2D directional CSMLTs and its corresponding 2D directional basis functions after the operation are shown in Fig. 5. Although the scaling coefficient $1/\sqrt{2}$ has been omitted in the equations, it is actually required for 2D directional CSMLTs to be a tight frame, i.e., energy preserving transform.

III. Nonexpansive Convolution for CSMLTs and CSMBTs

When a lapped transform is applied to an image, a nonexpansive convolution should be used at the boundaries not to increase the number of samples. In particular, SE is often used to avoid discontinuities at the boundaries. However, when SE is used on directional lapped transforms such as CSMLTs, directional discontinuities appear and the boundaries are distorted by annoying boundary artifacts in image restoration.

Here, we derive an efficient nonexpansive convolution for CSMLTs. Tanaka et al. devised a SE for nonlinear-phase

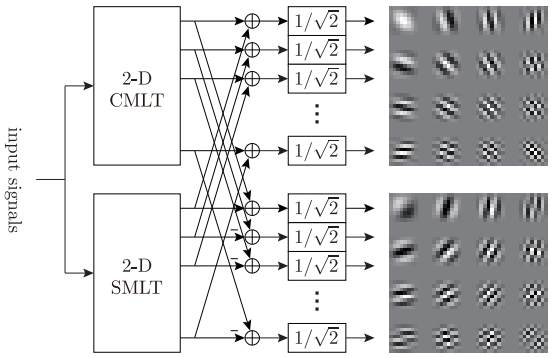

Fig. 5: Construction of $M\times 2KM$ CSMLTs and corresponding 2D directional basis functions of 4×8 CSMLTs.

paraunitary FBs (NLPPUFBs); they used a boundary filtering technique [27]. We will extend this idea to our nonexpansive convolution. Moreover, we propose new directional block transforms, called CSMBTs, derived from $M \times 2M$ CSMLTs with the nonexpansive convolutions.

A. Nonexpansive Convolution for CSMLTs

Here, we develop a nonexpansive convolution by boundary filtering for CMLT in accordance with [27]. The derivation for SMLT is omitted because it can be verified in the same way.

Fig. 6 shows the upper boundary processing in the case of $K = 1$ and 2. The boundary signals are generated by using a boundary extension matrix $\boldsymbol{\mathcal{E}}_{\frac{M}{2}}$, e.g., $\boldsymbol{\mathcal{E}}_{\frac{M}{2}} = \mathbf{J}_{\frac{M}{2}}$ in the case of SE. Given an arbitrary K, the upper and lower input signals require $(2K-1)M$ extra signals because of the filter length $L = 2KM$ for CSMLTs. We will show derivations for two cases, i.e., $K = 1$ and 2; we can easily handle the cases of $K \geq 3$ in a similar way by solving simultaneous matrix equations.

1) Case of $K = 1$: Signal reconstruction in the case of $K = 1$ is achieved with M extra signals in total. We consider the case of the boundary processing when reconstructing $\mathbf{x}_0$ from $\mathbf{a}_0$ at the top-right of Fig. 6. At the top-left of Fig. 6, the signal $\mathbf{a}_0$ is calculated as

$$\mathbf{a}_0 = \begin{bmatrix} [\boldsymbol{\Xi}_0]_\gamma \boldsymbol{\mathcal{E}} & [\boldsymbol{\Xi}_0]_\delta \end{bmatrix} \begin{bmatrix} \mathbf{x}_0 \\ \mathbf{x}_0 \end{bmatrix}, \tag{24}$$

where $\boldsymbol{\Xi}_0$ is in (17) and $\boldsymbol{\mathcal{E}}$ is an arbitrary $\frac{M}{2} \times \frac{M}{2}$ boundary extension matrix. We solve for $\mathbf{x}_0$ as follows:

$$\mathbf{x}_0 = \boldsymbol{\mathcal{U}}_0^{-1} \mathbf{a}_0, \tag{25}$$

where

$$\boldsymbol{\mathcal{U}}_0 = [\boldsymbol{\Xi}_0]_\gamma \boldsymbol{\mathcal{E}} + [\boldsymbol{\Xi}_0]_\delta .$$

In design of the CSMLTs, the coefficients in $\boldsymbol{\Xi}_0$ are heuristically chosen such that $\det(\boldsymbol{\mathcal{U}}_0) \neq 0$. The lower boundaries can be calculated in the same way as the upper boundaries.

2) Case of $K = 2$: Signal reconstruction in the case of $K = 2$ is achieved with $3M$ extra signals in total. Since the delay elements of CSMLTs in $K \geq 2$ are z^{-2} unlike z^{-1} in NLPPUFBs, we have to recalculate the boundary processing in $K \geq 2$. At the bottom-right of Fig. 6, we reconstruct $\mathbf{x}_0$, $\mathbf{x}_1$, and $\mathbf{x}_2$. $\mathbf{x}_1$ and $\mathbf{x}_2$ are reconstructed from $\mathbf{b}_0$ and $\mathbf{b}_5$ as

$$\begin{bmatrix} \mathbf{x}_1 \\ \mathbf{x}_2 \end{bmatrix} = \boldsymbol{\Xi}_1^\top \begin{bmatrix} \mathbf{b}_0 \\ \mathbf{b}_5 \end{bmatrix}, \tag{26}$$

where $\boldsymbol{\Xi}_1$ is in (17). Although $\mathbf{b}_0$ is not directly available at the inverse transform side, we can compensate it as follows. At the forward transform side, $\mathbf{b}_1$ is calculated by

$$\mathbf{b}_1 = \begin{bmatrix} [\boldsymbol{\Xi}_1]_\gamma \boldsymbol{\mathcal{E}} & [\boldsymbol{\Xi}_1]_\delta \boldsymbol{\mathcal{E}} \end{bmatrix} \begin{bmatrix} \mathbf{x}_2 \\ \mathbf{x}_1 \end{bmatrix}. \tag{27}$$

Accordingly, we substitute (26) in (27), from which (27) is calculated as

$$\mathbf{b}_1 = \begin{bmatrix} [\boldsymbol{\Xi}_1]_\delta \boldsymbol{\mathcal{E}} & [\boldsymbol{\Xi}_1]_\gamma \boldsymbol{\mathcal{E}} \end{bmatrix} \boldsymbol{\Xi}_1^\top \begin{bmatrix} \mathbf{b}_0 \\ \mathbf{b}_5 \end{bmatrix}. \tag{28}$$

On the other hand, $\mathbf{a}_0$ at the forward transform side is calculated as

$$\mathbf{a}_0 = \begin{bmatrix} [\boldsymbol{\Theta}_0]_\gamma & [\boldsymbol{\Theta}_0]_\delta \end{bmatrix} \begin{bmatrix} \mathbf{b}_0 \\ \mathbf{b}_1 \end{bmatrix}. \tag{29}$$

Therefore, at the inverse transform side, $\mathbf{b}_0$ can be calculated by solving the simultaneous matrix equation with (28) and (29). We obtain

$$\mathbf{b}_0 = \boldsymbol{\mathcal{V}}_0^{-1} \left(\mathbf{a}_0 - \boldsymbol{\mathcal{W}}_0 \mathbf{b}_5 \right), \tag{30}$$

where

$$\boldsymbol{\mathcal{V}}_0 = [\boldsymbol{\Theta}_0]_\delta \left([\boldsymbol{\Xi}_1]_\delta \boldsymbol{\mathcal{E}} [\boldsymbol{\Xi}_1]_\alpha^\top + [\boldsymbol{\Xi}_1]_\gamma \boldsymbol{\mathcal{E}} [\boldsymbol{\Xi}_1]_\beta^\top \right) + [\boldsymbol{\Theta}_0]_\gamma ,$$

$$\boldsymbol{\mathcal{W}}_0 = [\boldsymbol{\Theta}_0]_\delta \left([\boldsymbol{\Xi}_1]_\delta \boldsymbol{\mathcal{E}} [\boldsymbol{\Xi}_1]_\gamma^\top + [\boldsymbol{\Xi}_1]_\gamma \boldsymbol{\mathcal{E}} [\boldsymbol{\Xi}_1]_\delta^\top \right).$$

As for $\mathbf{x}_0$, we can reconstruct from the same discussion explained in the case of $K = 1$:

$$\mathbf{x}_0 = \boldsymbol{\mathcal{U}}_1^{-1} \mathbf{b}_3, \tag{31}$$

where

$$\boldsymbol{\mathcal{U}}_1 = [\boldsymbol{\Xi}_1]_\gamma \boldsymbol{\mathcal{E}} + [\boldsymbol{\Xi}_1]_\delta .$$

Similar to the case of $K = 1$, the coefficients are heuristically chosen in design such that $\det(\boldsymbol{\mathcal{U}}_1) \neq 0$ and $\det(\boldsymbol{\mathcal{V}}_0) \neq 0$. The lower boundaries can be calculated in the same way as the upper boundaries.

B. Mean Value Extension (MVE)

Before introducing MVE, we should confirm that the conventional extension methods are inefficient for directional textures. Figs. 7(b) and (c) show the results of PE and SE for the input image in Fig. 7(a). Since PE extends the directional textures at the boundaries along different directions, severe discontinuities appear. Although SE can extend them smoothly in terms of 1D signals, reflected (inverse) directional textures appear at the boundaries.

To reduce the directional discontinuities, we propose a more appropriate boundary extension matrix $\boldsymbol{\mathcal{E}}$ for CSMLTs. Because of the separable implementation, not all of the directional textures can be extended smoothly. Because of that,

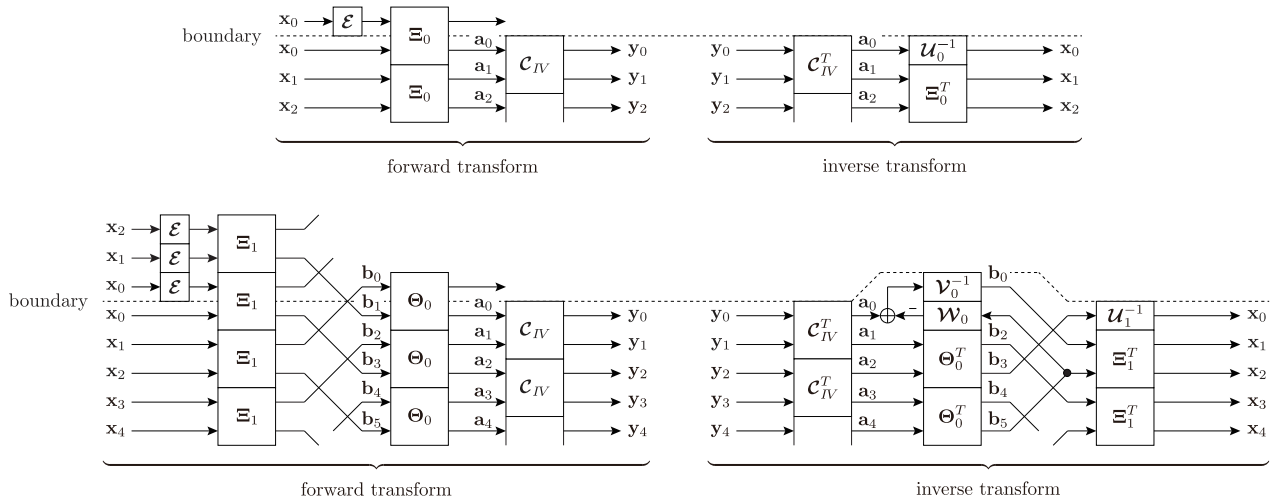

Fig. 6: Upper boundary processing of M-band CMLTs (each arrow indicates $M/2$ input signals): (top) $K = 1$; (bottom) $K = 2$.

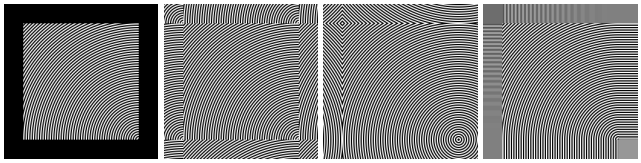

(a) (b) (c) (d)

Fig. 7: Boundary extensions: (a) original image (zero extension), (b) PE, (c) SE, and (d) MVE.

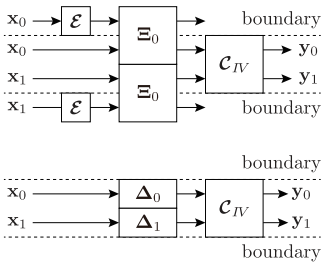

Fig. 8: Minimum tiling of CMLT: (top) without a nonexpansive convolution; (bottom) with a nonexpansive convolution.

we use the mean values of signals at the boundaries; i.e., the MVE matrix $\boldsymbol{\mathcal{E}}$ is given by

$$\boldsymbol{\mathcal{E}} = \frac{2}{M}\mathbf{1}_{\frac{M}{2}\times\frac{M}{2}}, \tag{32}$$

where $\mathbf{1}_{\frac{M}{2}\times\frac{M}{2}}$ is an $\frac{M}{2}\times\frac{M}{2}$ matrix with 1s in every element. As shown in Fig. 7(d), MVE can extend the lines at each boundary more smoothly so that severe directional discontinuities do not appear.

C. Cosine-Sine Modulated Block Transforms (CSMBTs)

Block transforms are used more than lapped transforms in small-scale embedded systems to keep down computational costs and gain benefit from parallel computation, e.g., they are used in image and video coding standards such as JPEG and the H.26x series. Here, we present new $M\times M$ directional block transforms, called CSMBTs. They can be derived from a minimum tiling of $M\times 2M$ CSMLTs, i.e., the case of $K=1$ in Section III-A1, and the nonexpansive convolutions. Note that the CSMBTs cannot be obtained when $K\geq 2$ because the minimum tile size is always bigger than M.

The CMLT with the nonexpansive convolution when $K=1$ for input signals longer than M is expressed as

$$\begin{aligned}&\operatorname{diag}\left(\boldsymbol{\mathcal{C}}_{IV},\boldsymbol{\mathcal{C}}_{IV},\cdots,\boldsymbol{\mathcal{C}}_{IV}\right)\\ &\times\ \operatorname{diag}\left(\mathbf{J}\mathbf{C}_0\boldsymbol{\mathcal{E}}+\mathbf{J}\mathbf{S}_0\mathbf{J},\boldsymbol{\Xi}_0,\boldsymbol{\Xi}_0,\cdots,\boldsymbol{\Xi}_0,-\mathbf{C}_0\mathbf{J}\boldsymbol{\mathcal{E}}+\mathbf{S}_0\right).\end{aligned} \tag{33}$$

When the size of input signals is M, i.e., the minimum tiling, (33) takes the following form (see the bottom of Fig. 8):

$$\mathbf{B}_{\mathcal{C}} = \boldsymbol{\mathcal{C}}_{IV}\begin{bmatrix}\mathbf{J}\mathbf{C}_0\boldsymbol{\mathcal{E}}+\mathbf{J}\mathbf{S}_0\mathbf{J} & \mathbf{O}\\ \mathbf{O} & -\mathbf{C}_0\mathbf{J}\boldsymbol{\mathcal{E}}+\mathbf{S}_0\end{bmatrix}. \tag{34}$$

It is clear that $\mathbf{B}_{\mathcal{C}}$ is an $M\times M$ block transform; we thus term it the cosine modulated block transform (CMBT). An $M\times M$ sine modulated block transform (SMBT) based on $M\times 2M$ SMLT is similarly obtained as

$$\mathbf{B}_{\mathcal{S}} = \boldsymbol{\mathcal{S}}_{IV}\begin{bmatrix}-\mathbf{J}\mathbf{C}_0\boldsymbol{\mathcal{E}}+\mathbf{J}\mathbf{S}_0\mathbf{J} & \mathbf{O}\\ \mathbf{O} & \mathbf{C}_0\mathbf{J}\boldsymbol{\mathcal{E}}+\mathbf{S}_0\end{bmatrix}. \tag{35}$$

Finally, the 2D directional CSMBTs are constructed by using the CMBT and SMBT instead of the CMLT and SMLT in Fig. 5. The Appendix shows a concrete numerical example of the relationship between 4×8 CSMLTs and 4×4 CSMBTs with MVE.

Remark: When the boundary extension matrix $\boldsymbol{\mathcal{E}}$ is a centrosymmetric matrix that satisfies $\boldsymbol{\mathcal{E}}\mathbf{J}=\mathbf{J}\boldsymbol{\mathcal{E}}$, such as SE and MVE matrices, SMBT $\mathbf{B}_{\mathcal{S}}$ has a simple relationship with CMBT $\mathbf{B}_{\mathcal{C}}$:

$$\begin{aligned}\mathbf{B}_{\mathcal{S}} &= \mathbf{D}\boldsymbol{\mathcal{C}}_{IV}\mathbf{J}\begin{bmatrix}\mathbf{J}\boldsymbol{\Delta}_1\mathbf{J} & \mathbf{O}\\ \mathbf{O} & \mathbf{J}\boldsymbol{\Delta}_0\mathbf{J}\end{bmatrix} = \mathbf{D}\boldsymbol{\mathcal{C}}_{IV}\begin{bmatrix}\boldsymbol{\Delta}_0 & \mathbf{O}\\ \mathbf{O} & \boldsymbol{\Delta}_1\end{bmatrix}\mathbf{J}\\ &= \mathbf{D}\mathbf{B}_{\mathcal{C}}\mathbf{J},\end{aligned} \tag{36}$$

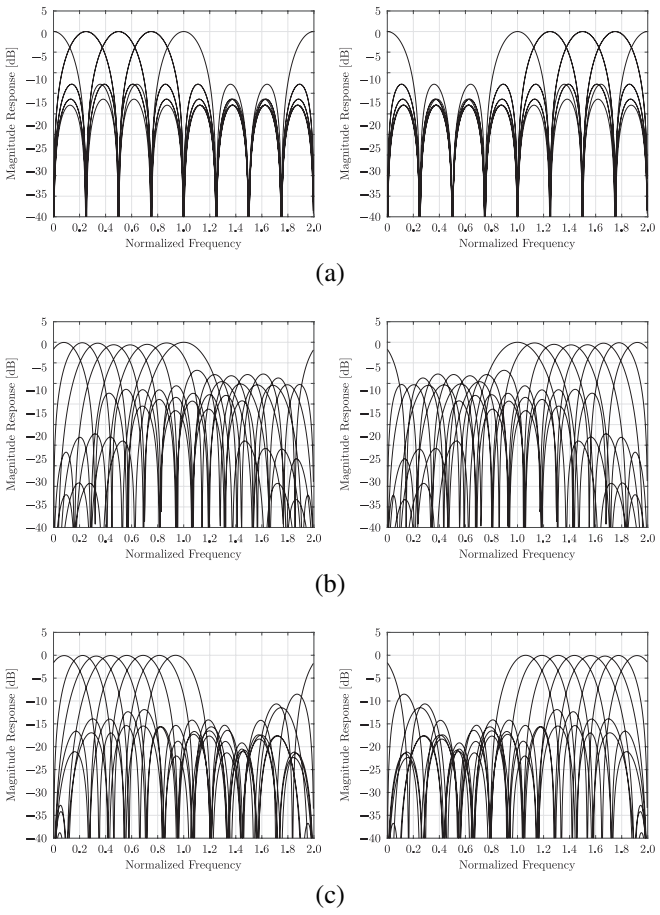

Fig. 9: Frequency responses of 8×8 CSMBTs ($[0, 2\pi]$): (a) PE, (b) SE, and (c) MVE: (left) $H_m(\omega) + jH'_m(\omega)$; (right) $H_m(\omega) - jH'_m(\omega)$, where $m \in \{0, 1, \cdots, 7\}$.

where

$$\boldsymbol{\Delta}_0 = \mathbf{J}\mathbf{C}_0\boldsymbol{\mathcal{E}} + \mathbf{J}\mathbf{S}_0\mathbf{J}$$
$$\boldsymbol{\Delta}_1 = -\mathbf{C}_0\mathbf{J}\boldsymbol{\mathcal{E}} + \mathbf{S}_0.$$

This relationship is the same as that holds between DCT-IV and DST-IV, $\boldsymbol{\mathcal{S}}_{IV} = \mathbf{D}\boldsymbol{\mathcal{C}}_{IV}\mathbf{J}$.

IV. Experimental Results

This section evaluates the CSMLTs and CSMBTs with PE, SE, and MVE. The resulting transforms were compared in terms of the peak signal-to-noise ratio (PSNR) [dB]:

$$\mathrm{PSNR[dB]} = 10\log_{10}\left(\frac{\left(2^{\mathrm{BIT}}-1\right)^2}{\mathrm{MSE}}\right),$$

where BIT and MSE are the image's bit-depth and mean squared error, respectively. The image set included 512×512 8-bit standard grayscale images in [34] such as *Barbara*, *Goldhill*, and *Lena*.

A. Filter Design

We designed 8×16 and 8×32 CSMLTs by using the cost function, which is a weighted linear combination of the coding gain and the DC leakage [35], and `fminunc.m` in `Optimization ToolBox` of `MATLAB`. Moreover, we derived 8×8 CSMBTs from 8×16 CSMLTs with nonexpansive convolutions, which are PE, SE, and MVE. In this section, the CSMLTs and CSMBTs with PE, SE, and MVE are labeled CSMLTs-PE, CSMLTs-SE, CSMLTs-MVE, CSMBTs-PE, CSMBTs-SE, and CSMBTs-MVE.

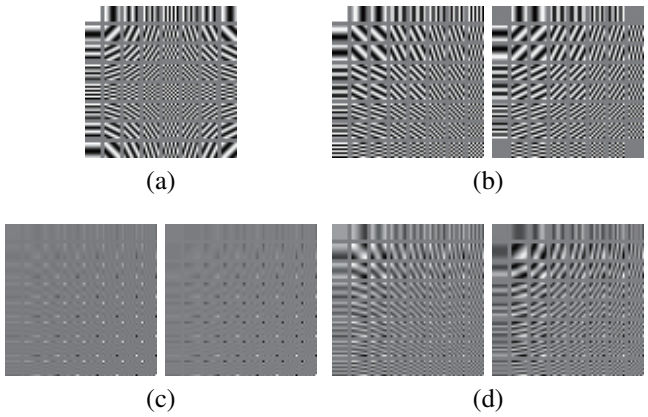

Fig. 10: 2D directional basis functions of 8×8 block transforms: (a) DFT, (b) CSMBTs-PE, (c) CSMBTs-SE, and (d) CSMBTs-MVE.

The complex combinations of the frequency responses and 2D directional basis functions of the 8×8 directional block transforms are shown in Figs. 9 and 10, respectively. Although the spectra based on CSMBTs-PE in Fig. 9(a) are one-sided in the positive or negative domain, as are the CSMLTs in Fig. 4(a), some spectra are completely duplicated. Thus, the resulting atoms from the CSMBTs-PE contain duplicate directional ones, as shown in Fig. 10(b). On the other hand, whereas none of the spectra based on CSMBTs-SE (Fig. 9(b)) are duplicated, they do not sufficiently attenuate in each stopband. Therefore, as shown in Fig. 10(c), each atom cannot distinguish the corresponding direction accurately. By contrast, the spectra from the CSMBTs-MVE are not duplicated and sufficiently attenuate in each stopband; the resulting atoms have richer directional selectivity than the others.

B. Non-linear Approximation (NLA)

We applied the CSMLTs, CSMBTs, and DFT to the non-linear approximation (NLA) [36], which is often used as a criterion for efficiency of sparse representation. Fig. 11 shows the rate-distortion (R-D) curves of NLA. The CSMLTs-MVE and CSMBTs-MVE achieved the best performance in every case. The top images of Figs. 12 and 13 show particular areas of *Barbara* and *Lena* in NLA (coefficient $= 4000$). The PE/SE-based directional transforms generated annoying artifacts, such as boundary artifacts, directional block artifacts, and black/white block artifacts, whereas CSMLTs-MVE and CSMBTs-MVE did not generate any.

C. Image Denoising

We also compared the CSMLTs, CSMBTs, and DFT by applying them to image denoising. Noisy images were made by adding Gaussian random noise with a standard deviation

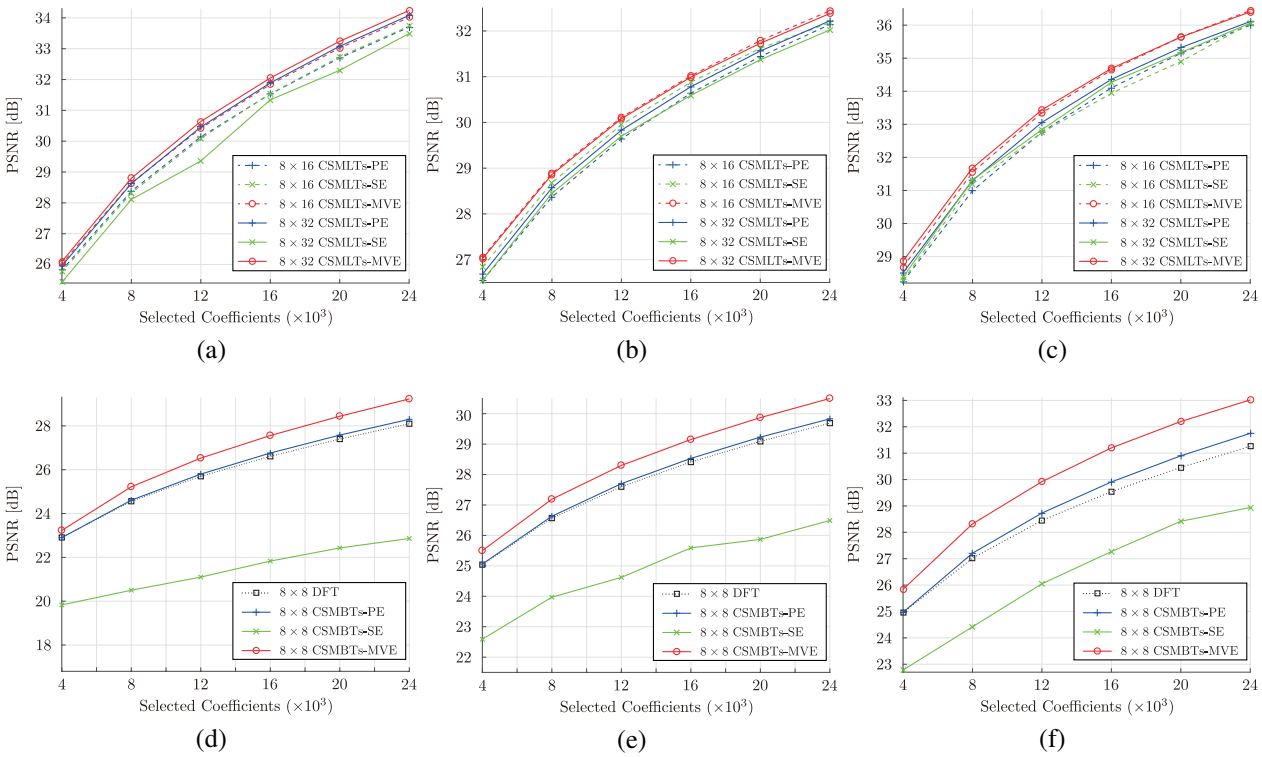

Fig. 11: R-D curves of NLA: (a-c) CSMLTs, (d-f) CSMBTs, (a,d) *Barbara*, (b,e) *Goldhill*, and (c,f) *Lena*.

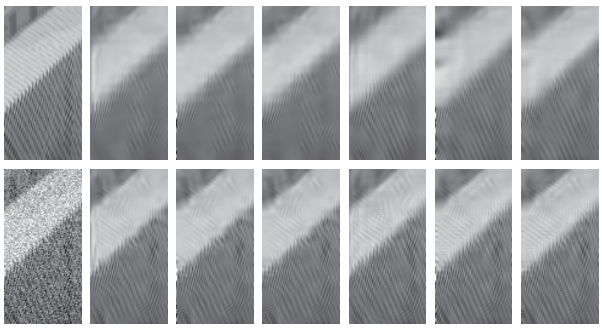

Fig. 12: Particular areas (left sides are boundaries) of *Barbara* in NLA (coefficients $= 4000$) and image denoising ($\sigma = 30$) by CSMLTs: (top) NLA, (bottom) image denoising, (left-to-right) original/noisy images, 8×16 CSMLTs-PE, 8×16 CSMLTs-SE, 8×16 CSMLTs-MVE, 8×32 CSMLTs-PE, 8×32 CSMLTs-SE, and 8×32 CSMLTs-MVE.

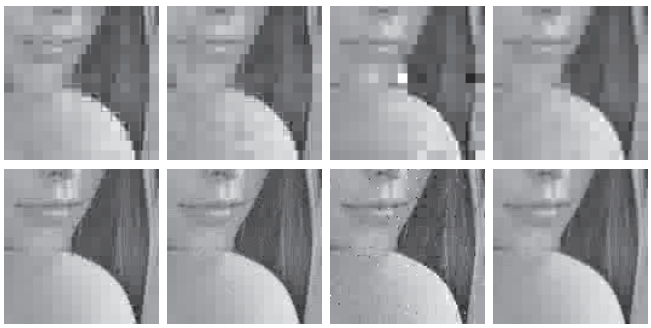

Fig. 13: Particular areas of *Lena* in NLA (coefficients $= 4000$) and image denoising ($\sigma = 10$) by 8×8 directional block transforms: (top) NLA, (bottom) image denoising, (left-to-right) DFT, CSMBTs-PE, CSMBTs-SE, and CSMBTs-MVE.

σ to the original images. The images were denoised by applying a universal threshold $\sigma\sqrt{2 \log N}$ [37], where N is the number of pixels, after the transforms had been performed. Fig. 14 shows the R-D curves of image denoising. CSMLTs-MVE and CSMBTs-MVE performed the best in almost all cases. Moreover, the bottom images of Figs. 12 and 13 show particular areas of *Barbara* and *Lena* in image denoising ($\sigma = 30$ and 10). Similar to the case of NLA, the PE/SE-based directional transforms generated annoying artifacts, but CSMLTs-MVE and CSMBTs-MVE did not generate any.

V. Conclusion

We proposed a new nonexpansive convolution, MVE, for CSMLTs. The conventional boundary extension methods, PE and SE, often produce directional discontinuities at boundaries, which degrade the efficiency of a sparse representation created by using a directional lapped transform. MVE reduces directional discontinuities by using the mean value of the pixels near the boundaries. We also devised new directional block transforms, called CSMBTs, derived from the minimum tiling of the CSMLTs with a $2M$ filter length and the nonexpansive convolutions. The resulting CSMBTs-MVE not only have rich directional selectivity at a low cost but also better mitigate annoying artifacts in NLA and image denoising compared with the DFT.

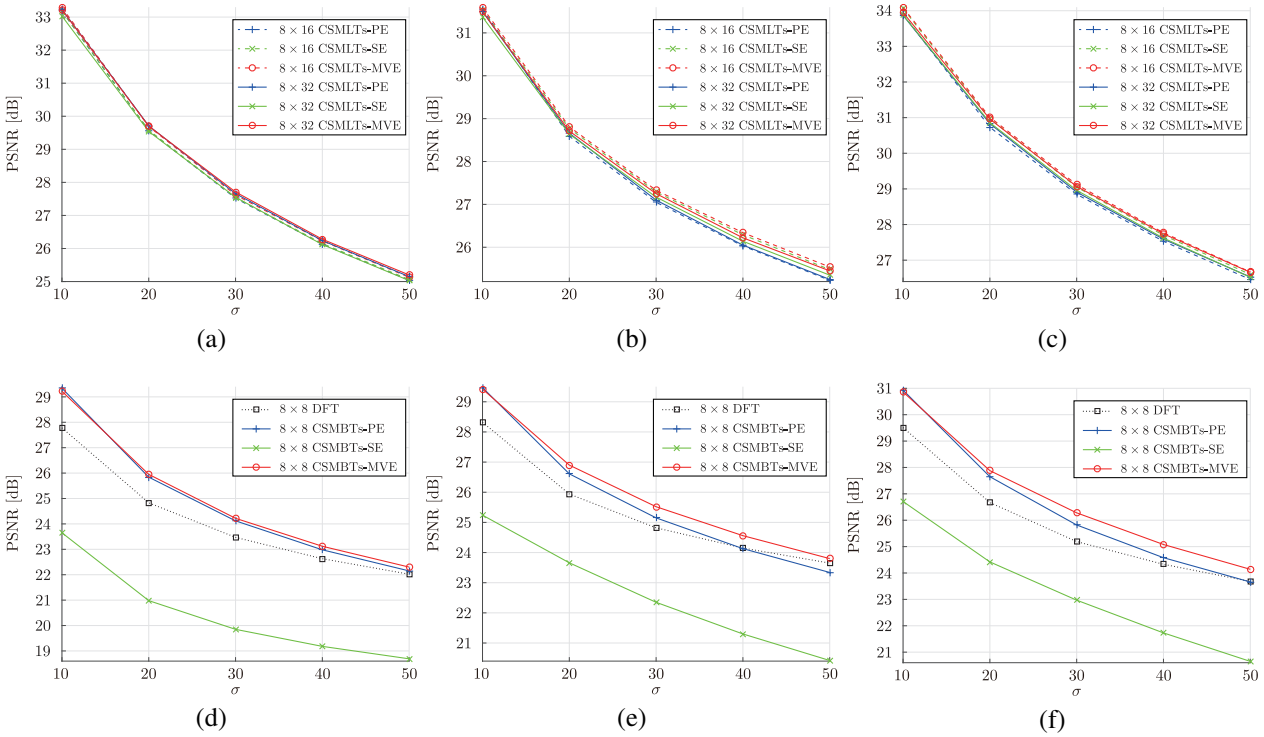

Fig. 14: R-D curves of image denoising: (a-c) CSMLTs, (d-f) CSMBTs, (a,d) *Barbara*, (b,e) *Goldhill*, and (c,f) *Lena*.

APPENDIX
A CONCRETE NUMERICAL EXAMPLE OF RELATIONSHIP BETWEEN CSMLTS AND CSMBTS WITH MVE

This Appendix shows a concrete numerical example of relationship between 4×8 CSMLTs and 4×4 CSMBTs with MVE. The resulting transforms are shown in Table I. We consider a pseudo-random 4×4 input block $\mathbf{x}$ as

$$\mathbf{x} = \begin{bmatrix} 3 & 1 & 4 & 1 \\ 5 & 9 & 2 & 6 \\ 5 & 3 & 5 & 8 \\ 9 & 7 & 9 & 3 \end{bmatrix} \tag{37}$$

and the 8×8 MVE-based extended block $\mathbf{x}'$ as

$$\mathbf{x}' = \begin{bmatrix} 4.5 & 4.5 & 4 & 5 & 3 & 3.5 & 3.25 & 3.25 \\ 4.5 & 4.5 & 4 & 5 & 3 & 3.5 & 3.25 & 3.25 \\ 2 & 2 & 3 & 1 & 4 & 1 & 2.5 & 2.5 \\ 7 & 7 & 5 & 9 & 2 & 6 & 4 & 4 \\ 4 & 4 & 5 & 3 & 5 & 8 & 6.5 & 6.5 \\ 8 & 8 & 9 & 7 & 9 & 3 & 6 & 6 \\ 6 & 6 & 7 & 5 & 7 & 5.5 & 6.25 & 6.25 \\ 6 & 6 & 7 & 5 & 7 & 5.5 & 6.25 & 6.25 \end{bmatrix}. \tag{38}$$

When 4×8 CSMLTs and 4×4 CSMBTs are applied to $\mathbf{x}'$ and $\mathbf{x}$, we obtain the 2D transformed coefficients as

$$\begin{aligned} &\begin{bmatrix} \mathbf{E}_{\mathcal{C}0} & \mathbf{E}_{\mathcal{C}1} \end{bmatrix} \mathbf{x}' \begin{bmatrix} \mathbf{E}_{\mathcal{C}0} & \mathbf{E}_{\mathcal{C}1} \end{bmatrix}^\top = \mathbf{B}_{\mathcal{C}} \mathbf{x} \mathbf{B}_{\mathcal{C}}^\top \\ &= \begin{bmatrix} 17.2762 & 0.8656 & -0.5848 & -1.4899 \\ -3.5692 & -0.0174 & -0.6653 & 1.2170 \\ -1.5671 & -0.7004 & 1.3007 & 4.5910 \\ -5.3497 & -1.2981 & 2.7250 & -0.0447 \end{bmatrix} \triangleq \mathbf{y}_{\mathcal{C}} \end{aligned} \tag{39}$$

$$\begin{aligned} &\begin{bmatrix} \mathbf{E}_{\mathcal{S}0} & \mathbf{E}_{\mathcal{S}1} \end{bmatrix} \mathbf{x}' \begin{bmatrix} \mathbf{E}_{\mathcal{S}0} & \mathbf{E}_{\mathcal{S}1} \end{bmatrix}^\top = \mathbf{B}_{\mathcal{S}} \mathbf{x} \mathbf{B}_{\mathcal{S}}^\top \\ &= \begin{bmatrix} 23.2061 & 0.3670 & -0.1711 & 1.4449 \\ -2.6012 & -1.0096 & 2.2133 & -3.1325 \\ -1.9793 & 2.9281 & -2.0320 & 0.8948 \\ -1.6648 & -2.3473 & -1.3771 & 4.0055 \end{bmatrix} \triangleq \mathbf{y}_{\mathcal{S}}, \end{aligned} \tag{40}$$

respectively. They mean that the CSMBTs with MVE are exactly the same as a minimum tiling of the CSMLTs with MVE. Note that the resulting output signals in the 2D directional transforms are $(\mathbf{y}_{\mathcal{C}} + \mathbf{y}_{\mathcal{S}})/\sqrt{2}$ and $(\mathbf{y}_{\mathcal{C}} - \mathbf{y}_{\mathcal{S}})/\sqrt{2}$.

ACKNOWLEDGMENT

The authors would like to thank the anonymous reviewers for providing many constructive suggestions that significantly improve the presentation of this paper. This work was supported by Grant-in-Aids for Young Scientists (B), Grant Number 16K18100 and 17K14683, from the Japan Society for the Promotion of Science (JSPS).

REFERENCES

[1] K. R. Rao and P. Yip, *Discrete Cosine Transform Algorithms*, Academic Press, 1990.

TABLE I: Concrete filter coefficients of resulting transforms ($M = 4$).

Resulting Transforms	Filter Coefficients
4×8 CMLT $\mathbf{E}_{\mathcal{C}}(z)$	$\underbrace{\begin{bmatrix} 0.1147 & 0.3853 & 0.5766 & 0.5766 \\ -0.0269 & 0.3266 & 0.4889 & -0.1353 \\ -0.1353 & 0.2183 & 0.3266 & -0.6802 \\ -0.0766 & 0.0766 & 0.1147 & -0.3853 \end{bmatrix}}_{\triangleq \mathbf{E}_{\mathcal{C}0}} + \underbrace{\begin{bmatrix} 0.3853 & 0.1147 & -0.0766 & -0.0766 \\ -0.6802 & -0.3266 & 0.2183 & 0.1353 \\ 0.1353 & 0.4889 & -0.3266 & -0.0269 \\ 0.5766 & -0.5766 & 0.3853 & -0.1147 \end{bmatrix}}_{\triangleq \mathbf{E}_{\mathcal{C}1}} z^{-1}$
4×8 SMLT $\mathbf{E}_{\mathcal{S}}(z)$	$\underbrace{\begin{bmatrix} 0.0766 & 0.0766 & -0.1147 & -0.3853 \\ 0.1353 & 0.2183 & -0.3266 & -0.6802 \\ 0.0269 & 0.3266 & -0.4889 & -0.1353 \\ -0.1147 & 0.3853 & -0.5766 & 0.5766 \end{bmatrix}}_{\triangleq \mathbf{E}_{\mathcal{S}0}} + \underbrace{\begin{bmatrix} -0.5766 & -0.5766 & -0.3853 & -0.1147 \\ -0.1353 & 0.4889 & 0.3266 & -0.0269 \\ 0.6802 & -0.3266 & -0.2183 & 0.1353 \\ -0.3853 & 0.1147 & 0.0766 & -0.0766 \end{bmatrix}}_{\triangleq \mathbf{E}_{\mathcal{S}1}} z^{-1}$
4×4 CMBT $\mathbf{B}_{\mathcal{C}}$	$\begin{bmatrix} 0.8266 & 0.8266 & 0.3087 & 0.0381 \\ 0.6387 & 0.0146 & -0.5034 & -0.1499 \\ 0.3681 & -0.6387 & -0.0415 & 0.3121 \\ 0.1147 & -0.3853 & 0.7119 & -0.4413 \end{bmatrix}$
4×4 SMBT $\mathbf{B}_{\mathcal{S}}$	$\begin{bmatrix} 0.0381 & 0.3087 & 0.8266 & 0.8266 \\ 0.1499 & 0.5034 & -0.0146 & -0.6387 \\ 0.3121 & -0.0415 & -0.6387 & 0.3681 \\ 0.4413 & -0.7119 & 0.3853 & -0.1147 \end{bmatrix}$

[2] G. Strang and T. Nguyen, *Wavelets and Filter Banks*, Wellesley-Cambridge Press, 1996.

[3] G. K. Wallace, "The JPEG still picture compression standard," *IEEE Trans. Consum. Electr.*, vol. 38, no. 1, pp. xviii–xxxiv, Feb. 1992.

[4] T. Wiegand, G. J. Sullivan, G. Bjøntegaard, and A. Luthra, "Overview of the H.264/AVC video coding standard," *IEEE Trans. Circuits Syst. Video Technol.*, vol. 13, no. 7, pp. 560–576, July 2003.

[5] G. J. Sullivan, J.-R. Ohm, W.-J. Han, and T. Wiegand, "Overview of the high efficiency video coding (HEVC) standard," *IEEE Trans. Circuits Syst. Video Technol.*, vol. 22, no. 12, pp. 1649–1668, Dec. 2012.

[6] A. Skodras, C. Christopoulis, and T. Ebrahimi, "The JPEG2000 still image compression standard," *IEEE Signal Process. Mag.*, vol. 18, no. 5, pp. 36–58, Sep. 2001.

[7] I. W. Selesnick, R. G. Baraniuk, and N. C. Kingsbury, "The dual-tree complex wavelet transform," *IEEE Signal Process. Mag.*, vol. 22, no. 6, pp. 123–151, June 2005.

[8] W. Ding, F. Wu, X. Wu, and S. Li, "Adaptive directional lifting-based wavelet transform for image coding," *IEEE Trans. Image Process.*, vol. 16, no. 2, pp. 416–427, Feb. 2007.

[9] H. Xu, J. Xu, and F. Wu, "Lifting-based directional DCT-like transform for image coding," *IEEE Trans. Circuits Syst. Video Technol.*, vol. 17, no. 10, pp. 1325–1335, Oct. 2007.

[10] J. Xu, F. Wu, J. Liang, and W. Zhang, "Directional lapped transforms for image coding," *IEEE Trans. Image Process.*, vol. 19, no. 1, pp. 85–97, Jan. 2010.

[11] T. Yoshida, T. Suzuki, S. Kyochi, and M. Ikehara, "Two dimensional non-separable adaptive directional lifting structure of discrete wavelet transform," *IEICE Trans. Fundamentals.*, vol. E94-A, no. 10, pp. 1920–1927, Oct. 2011.

[12] F. A. B. Hamzah, T. Yoshida, M. Iwahashi, and H. Kiya, "Adaptive directional lifting structure of three dimensional non-separable discrete wavelet transform for high resolution volumetric data compression," *IEICE Trans. Fundamentals.*, vol. E99-A, no. 5, pp. 892–899, May 2016.

[13] J. L. Starck, E. J. Cand'es, and D. L. Donoho, "The curvelet transform for image denoising," *IEEE Trans. Image Process.*, vol. 11, no. 6, pp. 670–684, June 2002.

[14] M. N. Do and M. Vetterli, "The finite ridgelet transform for image representation," *IEEE Trans. Image Process.*, vol. 12, no. 1, pp. 16–28, Jan. 2003.

[15] M. N. Do and M. Vetterli, "The contourlet transform: An efficient directional multiresolution image representation," *IEEE Trans. Image Process.*, vol. 14, no. 12, pp. 2091–2106, Dec. 2005.

[16] S. Muramatsu, T. Kobayashi, M. Hiki, and H. Kikuchi, "Boundary operation of 2-D nonseparable linear-phase paraunitary filter banks," *IEEE Trans. Image Process.*, vol. 21, no. 4, pp. 2314–2318, Apr. 2012.

[17] S. Muramatsu, D. Han, T. Kobayashi, and H. Kikuchi, "Directional lapped orthogonal transform: Theory and design," *IEEE Trans. Image Process.*, vol. 21, no. 5, pp. 2434–2448, May 2012.

[18] S. Muramatsu, K. Furuya, and N. Yuki, "Multidimensional nonseparable oversampled lapped transforms: Theory and design," *IEEE Trans. Signal Process.*, vol. 65, no. 5, Mar. 2017.

[19] N. Ahmed and K. R. Rao, *Orthogonal Transforms for Digital Signal Processing*, Berlin, Germany: Springer-Verlag, 1975.

[20] I. W. Selesnick, "Hilbert transform pairs of wavelet bases," vol. 8, no. 6, pp. 170–173, June 2001.

[21] S. Kyochi, T. Uto, and M. Ikehara, "Dual-tree complex wavelet transform arising from cosine-sine modulated filter banks," in *Proc. of ISCAS'09*, Taipei, Taiwan, May 2009, pp. 2189–2192.

[22] S. Kyochi and M. Ikehara, "A class of near shift-invariant and orientation-selective transform based on delay-less oversampled even-stacked cosine-modulated filter banks," *IEICE Trans. Fundamentals.*, vol. E93-A, no. 4, pp. 724–733, Apr. 2010.

[23] L. Liang and H. Liu, "Dual-tree cosine-modulated filter bank with linearphase individual filters: An alternative shift-invariant and directional selective transform," *IEEE Trans. Image Process.*, vol. 22, no. 12, pp. 5168–5180, Dec. 2013.

[24] R. Ogawa, S. Kyochi, and T. Suzuki, "Design of oversampled cosine-sine modulated filter banks for directional image representation," in *Proc. of APSIPA ASC'15*, Hong Kong, Dec. 2015, pp. 370–373.

[25] H. S. Malvar, "A modulated complex lapped transform and its applications to audio processing," in *Proc. of ICASSP'99*, Phoenix, AZ, Mar. 1999, pp. 1421–1424.

[26] M. J. T. Smith and S. L. Eddins, "Analysis/synthesis techniques for subband image coding," *IEEE Trans. Signal Process.*, vol. 38, no. 8, pp. 1446–1456, Aug. 1990.

[27] Y. Tanaka, A. Ochi, and M. Ikehara, "A non-expansive convolution for nonlinear-phase paraunitary filter banks and its application to image coding," in *Proc. of ACSSC'05*, Pacific Grove, CA, Oct. 2005, pp. 54–58.

[28] T. Uto, T. Oka, and M. Ikehara, "M-channel nonlinear phase filter banks in image compression: Structure, design, and signal extension," *IEEE Trans. Signal Process.*, vol. 55, no. 4, pp. 1339–1351, Apr. 2007.

[29] T. Suzuki and M. Ikehara, "Reversible symmetric non-expansive convolution: An effective image boundary processing for M-channel lifting-based linear-phase filter banks," *IEEE Trans. Image Process.*, vol. 23, no. 6, pp. 2744–2749, June 2014.

[30] S. Kyochi, T. Suzuki, and Y. Tanaka, "A directional and shift-invariant transform based on M-channel rational-valued cosine-sine modulated filter banks," in *Proc. of APSIPA ASC'12*, Hollywood, CA, Dec. 2012, pp. 1–4.

[31] R. Ishibashi, T. Suzuki, S. Kyochi, and H. Kudo, "Image boundary extension with mean values for cosine-sine modulated filter banks," in *Proc. of ISCIT'15*, Nara, Japan, Oct. 2015, pp. 69–72.

[32] R. D. Koilpillai and P. P. Vaidyanathan, "Cosine-modulated FIR filter banks satisfying perfect reconstruction," *IEEE Trans. Signal Process.*, vol. 40, no. 4, pp. 770–783, Apr. 1992.

[33] H. S. Malvar, *Signal Processing with Lapped Transforms*, Norwood, MA: Artech House, 1992.

[34] "The USC-SIPI Image Database," *Univ. Southern California, Signal and Image Processing Institute [Online]*, Available: http://sipi.usc.edu/database/.

[35] P. P. Vaidyanathan, *Multirate Systems and Filter Banks*, Englewood Cliffs, NJ: Prentice Hall, 1992.
[36] S. Mallat, *A Wavelet Tour of Signal Processing: The Sparse Way*, Academic Press, 3rd edition, 2008.
[37] D. L. Donoho, "De-noising by soft-thresholding," *IEEE Trans. Inform. Theory*, vol. 41, no. 5, pp. 613–621, May 1995.

Ryoma Ishibashi graduated from the Advanced Production Systems Engineering Course, Gunma National College of Technology, Japan, and received the B.E. degree from the National Institution for Academic Degrees and University Evaluation, Japan, in 2014. He received the M.E. degree from the University of Tsukuba, Japan, in 2016. He joined NEC Corporation in 2016. His current research interests are signal/image processing and satellite communications.

Taizo Suzuki (S'08-M'11-SM'17) received the B.E., M.E., and Ph.D. degrees in electrical engineering from Keio University, Japan, in 2004, 2006 and 2010, respectively. From 2006 to 2008, he was with Toppan Printing Co., Ltd., Japan. From 2008 to 2011, he was a Research Associate of the Global Center of Excellence (G-COE) at Keio University, Japan. From 2010 to 2011, he was a Research Fellow of the Japan Society for the Promotion of Science (JSPS) and a Visiting Scholar at the Video Processing Group, the University of California, San Diego, CA. From 2011 to 2012, he was an Assistant Professor in the Department of Electrical and Electronic Engineering, College of Engineering, Nihon University, Japan. Since 2012, he has been an Assistant Professor in the Faculty of Engineering, Information and Systems, University of Tsukuba, Japan. His current research interests are image and video processing, source coding, and multidimensional transforms. Since 2017, he has been an Associate Editor of IEICE Trans. Fundamentals.

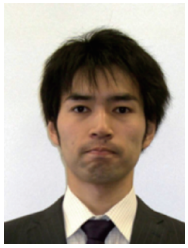

Seisuke Kyochi (S'08-M'10) received his B.S. in mathematics from Rikkyo University, Japan, in 2005 and his M.E. and Ph.D. from Keio University, Japan, in 2007 and 2010. He was a researcher at NTT Cyberspace Laboratories from 2010 to 2012. In 2012, he joined The University of Kitakyushu, and since 2015 he has been an Associate Professor of the Faculty of Environmental Engineering. His research interests include the theory and design of wavelets/filter banks for efficient image processing applications.

Hiroyuki Kudo (M'88) received the B.Sc. degree from the Department of Electrical Communications, Tohoku University, Japan, in 1985, and the Ph.D. degree from the Graduate School of Engineering, Tohoku University, in 1990. In 1992, he joined the University of Tsukuba, Japan, as an Assistant Professor. He is currently a Professor with the Division of Information Engineering, Faculty of Engineering, Information and Systems, University of Tsukuba, Japan. He is involved in tomographic image reconstruction for X-ray CT, PET, SPECT, and electron tomography. His research interests include medical imaging, image processing, and inverse problems. He is a member of the Japanese Society of Medical Imaging Technology and IEICE, Japan. He received the best paper award several times from various domestic and international academic societies. In particular, his papers on interior tomography published in 2008 were selected as Highlights of the two journals, Physics in Medicine and Biology and Inverse Problems. Since 2011, he has been Editor-in-Chief of the Journal of Medical Imaging Technology at MIT.